IEEE Access
Multidisciplinary | Rapid Review | Open Access Journal

Received 25 May 2023, accepted 20 June 2023, date of publication 10 July 2023, date of current version 20 July 2023.

Digital Object Identifier 10.1109/ACCESS.2023.3293756

RESEARCH ARTICLE

Evaluation of Effect of Pre-Processing Techniques in Solar Panel Fault Detection

SUJATA P. PATHAK, (Member, IEEE), AND SONALI A. PATIL
K. J. Somaiya College of Engineering, Somaiya Vidyavihar University (SVU), Vidyavihar, Mumbai 400077, India
Corresponding author: Sujata P. Pathak (sujatapathak@somaiya.edu)

ABSTRACT Solar energy is a clean and renewable source of energy produced by solar panels. Solar panels deteriorate over time, resulting in generation of faults. Faults reduce the overall power generation capacity of photovoltaic (PV) plants. A variety of atmospheric and functional conditions contribute to the formation of hotspots on solar panels, indicating an increase in temperature and resulting in lower efficiency. Early detection of faults during PV module inspection and monitoring is critical for improving the efficiency, reliability, and safety of PV systems. Thermal imaging is a non-contact, non-destructive, efficient, and effective technique. With thermal image analysis, probable problem areas can be identified and fixed before actual failures or problems occur, resulting in lower costs and less human labor. In this study, the effect of pre-processing techniques on fault detection in thermal images is studied and a comparative fault detection and demarcation method is proposed. Pre-processing is one of the steps in an automated fault detection system for removing noise or artefacts from thermal images. This study investigates the impact of pre-processing techniques such as filters and histogram equalization on fault detection and demarcation accuracy. Five different types of faults, such as single cell, multicell, diode, dust/shadow, and PID hotspot are detected. For fault detection, two segmentation techniques, histogram-based color thresholding and RGB color channel-based thresholding, are applied to thermal images of solar panels. Intersection over Union (IoU) is used to determine the efficiency of fault detection and demarcation techniques. Application of filters and histogram equalization on the dataset provided increased contrast and highlighted the faulty area of the thermal image more prominently. Overall, images processed with a bilateral filter and histogram equalization performed better for fault detection and demarcation than other filters. This technique resulted in IoU values of 0.35, 0.14, 0.31, 0.54 and 0.32 for diode, dust, multicell, single cell and PID hotspots respectively.

INDEX TERMS Photovoltaics, solar energy, thermal images, intersection over union, segmentation.

I. INTRODUCTION

Solar energy is the most affordable and fastest growing source of renewable energy. In an hour, the sun gives off more energy than the world consumes in one year. The most widely used solar technologies for businesses and homes are solar photovoltaics for electricity and solar water heating. A collection of PV modules is called a PV panel, and a system of PV panels is called an array. Arrays of a photovoltaic system supply solar electricity to electrical equipment. Solar panels are designed to give the maximum output when exposed to solar radiation. The working conditions of solar panels can be affected by atmospheric conditions like dirt, dust, the presence of foreign objects, shadowing, or functional conditions like cell mismatch or damage, string mismatch, winter shading, soiling, rooftop conditions, etc., which result in the generation of hotspots. Installation of panels at a height on the rooftop of buildings or over a larger area, makes the inspection process of individual PV panels significantly time consuming, complicated, and expensive. Fault detection and analysis are two of the most important parts of the operations and maintenance section.

Thermal imaging is a non-invasive and non-destructive method used for inspection of solar panels under load, so shutdown isn't required. Appropriate use of thermal imaging cameras shows accurate temperature differences between

The associate editor coordinating the review of this manuscript and approving it for publication was Byung-Gyu Kim.

This work is licensed under a Creative Commons Attribution-NonCommercial-NoDerivatives 4.0 License.
For more information, see https://creativecommons.org/licenses/by-nc-nd/4.0/

cells, which allows us to identify faults at an early stage. Thermal cameras capture raw thermal images, which contain important information used for image analysis. With thermal image analysis, problematic areas can be identified and repaired. Fault detection and classification are necessary for the efficiency, reliability, and safety of PV systems. One of the ways to improve PV array output is to ensure that the array operates in optimal output conditions at all times. Once installed, PV arrays are expected to operate with least human intervention. PV arrays perform below optimum output power levels due to faults in modules, wiring, inverter, and so forth [1]. Most of these faults remain undetected for a long period of time resulting in loss of power. Experts assigned to locate and fix the faults within an array need to take time consuming field measurements. Fault analysis in the solar PV arrays is a fundamental task to eliminate any kind of dangerous and undesirable situations arising in the operation of PV array due to the presence of faults [1], [2]. They must be detected and cleared off rapidly. Without proper fault detection, noncleared faults in PV arrays not only cause power losses but also might lead to safety issues and fire hazards [2], [3]

The primary objective of this proposed work is to study and investigate the effect of pre-processing technique on the accuracy of fault detection in solar panels. Image pre-processing involves removal of noise using selected filters and image enhancement. Faults are detected and located by applying two segmentation techniques on pre-processed images. Filtering and image enhancement using histogram equalization are applied on original thermal images. Various filters such as Mean, Median, Bilateral, and Gaussian are tested. Filtered images are enhanced using histogram equalization. Two segmentation techniques with histogram-based color thresholding and separate color channel-based thresholding are applied on pre-processed images. This paper contributes to detection of hotspots in thermal images of solar panels. Pre-processing of thermal images increases the accuracy of fault detection and demarcation. Detection and demarcation of hotspots at earlier stages with the help of thermal images helps in proper maintenance of solar panelsthereby increasing the generation of solar energy.

The structure of the rest of the paper is as follows. Section II explains the related work. Proposed methodology along with description of filters and histogram equalization techniques and dataset information is presented in section III. Section IV presents the results followed by discussion. Finally, the study conclusion is provided in section V.

II. RELATED WORK

Bharath Kurukuru et al. [4] have used Canny edge detection and Hough Transform technique for segmentation of faulty panel from a series of panels. From faulty panel, the features were extracted, and classification was done. Authors in [5] have used color thresholding in HSV space for RoI extraction. This segmented image was applied to Canny edge detection. Contours detected under certain thresholds are filtered resulting in a binary image having borders of PV modules. Dotenco et al. [6] modelled foreground in photovoltaic modules using a Gaussian distribution. To separate foreground from background, threshold was calculated from normalized temperature map. But due to high variance of background regions, it cannot be completely excluded from the foreground. Hence, the variance Tvar of the normalized temperature map Tnorm using a 3×3 kernel was used, which allowed region detection with high inconsistency and were probable to be part of the background. K-means algorithm was used to cluster the thermal image into many regions and identify the damaged area [7]. Additionally, to select the optimal number of clusters Elbow and gap methods were used with various values for Guerriero and Daliento [8] proposed segmentation method based on gradient analysis and edge detection. Edge detection method automatically selects the area in the thermal image related to the specific PV panel to be analyzed. Aghaei et al. [9] proposed the segmentation method to identify faulty panel using luminance of gray scale image of solar panel. Image is separated into black and white areas using threshold based on luminance and standard deviation of image. In the segmentation algorithm used by Kim et al. [10], panel boundaries were extracted with horizontal filtering, vertical filtering, and a modified tiered histogram clustering method. By applying an additional morphological algorithm, initial panel boundaries were obtained. With the geometry of surrounding panels, these extracted panel boundaries were refined by processing digital image in HSV color space. Kaplani [11] presented a method which automatically detects EVA discoloration in PV cells. Primarily based on hue, segmentation is applied in HSV color space. Regions with undefined hue are masked with saturation component. Next, with different tones of color in regions to detect different strengths of browning effect, value component is used. Authors [12] have extracted temperature information from thermal image such as average temperature, maximum temperature, and minimum temperature. Based on these values, threshold was selected. Count value was increased if the temperature value was less than high and low threshold. The module was considered an abnormal module if the count value exceeds 0.2% of the module area value. Gray scale image is converted into a binary image by selecting a grey level threshold in the original image by Tsanakas et al. [13]. Every pixel is converted into black or white according to its grey value whether it is greater or less than the threshold. An optimum threshold of 160 was selected that achieves a good separation of unwanted areas in most of the thermal images under testing, without removing any ROI. Combination of canny edge detection and color quantization has been used by Akram et al. [14] to segment defective regions in thermal images. For color quantization, k-means clustering was used with value of k=3. Authors [15] have used an algorithm consisting of image pre-processing, edge detection and segmentation. Edge detection with different threshold settings at different ranges is used to determine edges of filtered images. Contours that are evaluated in shape and size are

calculated at each edge detection step. At the end, to collect all the segmentations made, contours are drawn as a mask in an iterative way in an image. Segmentation based hot pixel detection algorithm is presented by Alsafasfeh et al. [16]. This method determines a hot pixel (seed pixel) in the input image for segmentation. After pre-processing the image, the value of the hottest pixel is determined by finding the highest pixel value. After this, all the neighboring pixels were checked if they are related to the hot pixel, called as seed pixels *SP*, or background pixels *BP*. Winston et al. [17] have used Feed Forward Back Propagation Neural Network technique and Support Vector Machine (SVM) technique to classify solar panel faults as micro-cracks and hotspots. Six input parameters like percentage of power loss (PPL), Irradiance (IRR), Open-circuit voltage (VOC), Short circuit current (ISC), Panel temperature and Internal impedance (Z) are used as input to these two classifiers.

To detect thermal defects in PV module infrared (IR) images were used and for detecting module surface defects, RGB images were used by authors Kuo et al. [18]. The combination of these two images were used were used to cross validate the reasons for module defects. For PV module and defect feature segmentation, Otsu algorithm is used. Image value change is used to define the optimal threshold value. Wang et al. [19] have proposed a combination of U-net and decision tree classifier for condition monitoring and fault diagnosis of PV panel. Image segmentation is done with the help of U-net neural network. Fault diagnosis using decision tree is based on the contour features in the 'mask' of true color infrared images. An ensemble-based deep neural network (DNN) model for detection of visual faults such as glass breakage, burn marks, snail trail, discoloration, and delamination on various PV modules is used by the authors [20]. Various features such as discrete wavelet transform (DWT), texture, grey level co-occurrence matrix (GLCM), fast Fourier transform (FFT), and grey level difference method (GLDM) are extracted from RGB images and applied as input to ensemble-based deep neural network (DNN) model. Onim et al. [21]. proposed a CNN architecture, SolNet, specifically for dust detection on solar panels. This proposed model is evaluated against current state-of-the-art (SOTA) algorithms for the same dust dataset.

By interpreting the methods mentioned in the previous work, it can be deduced that a major problem is availability of large dataset for solar panel thermal images. In the literature, work has been done on a small dataset. Faults are detected and localized using existing segmentation techniques. A lot of noise gets introduced due to environmental conditions during capturing of thermal images of solar panel. The goal of noise or artifact removal is to remove the noise without distorting the original image. Depending on the type of noise or artifact, different methods may be applied for pre-processing. There is a need to devise the right thermal image pre-processing strategy which leads to an increase in fault detection accuracy. Accurate detection of faults at earlier stage results in an increase of power generation capacity of solar plants.

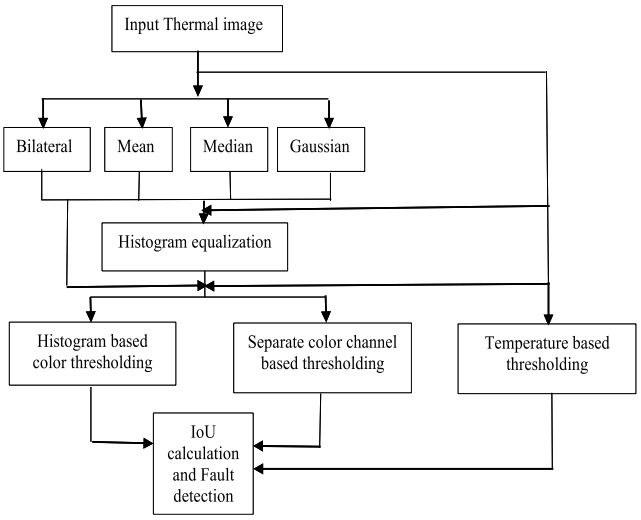

FIGURE 1. Proposed methodology.

TABLE 1. Dataset details.

Sr. No	Fault Type	No. of Images
1.	Diode fault	139
2.	Dust Shadow hotspot	39
3.	Single cell hotspot	807
4.	Multicell hotspot	210
5.	PID fault	311

III. METHODOLOGY

To test the effectiveness of pre-processing techniques, four filters like Mean [23], [24], [25], Median [11], [13], [14], [23], [24], [25], Bilateral [26] and Gaussian [9], [4], [11], [13] are applied on the thermal image. Filtered images are enhanced by applying histogram equalization.

The proposed method consists of image pre-processing, segmentation, and fault detection as major blocks. The detailed process is as shown in Fig. 1.

A. DATASET

FLIR C2 thermal camera is used to capture thermal images from various solar plants across India. These images are captured at different times and dates. The images are provided by PV Diagnostics, Mumbai, India.

Total number of images belonging to five different classes are shown in Table 1. Fig.2 shows sample images labelled by experts into five different classes as single cell hotspot, multicell hotspot, potentially induced degradation (PID) fault, diode fault and dust/shadow hotspot.

B. PRE-PROCESSING TECHNIQUES

The objective of pre-processing is to improve image data by suppressing unwilling distortions or to enhance some image features important for further processing. Four basic filters and histogram equalization technique used in this approach are detailed as below:

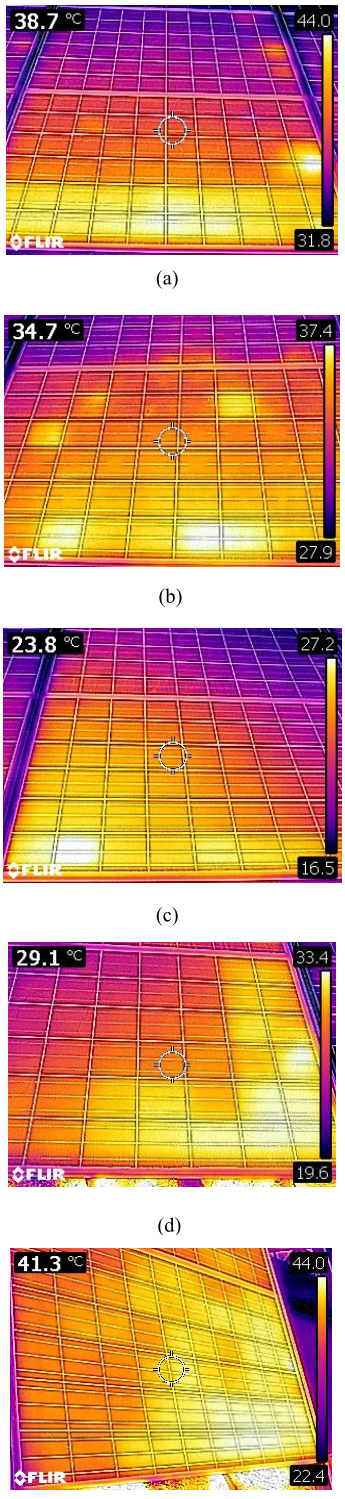

FIGURE 2. Various faults on solar panel (a)-diode fault, (b) Multicell hotspot, (c) Single cell hotspot, (d) PID fault, (e) Dust/Shadow Hotspot.

1) FILTERING

Filtering is a technique used for enhancing or modifying an image. An image is filtered to emphasize certain features or remove other features.

a: MEAN FILTER

Mean filtering, also called box filtering, is a basic and simple method often used for smoothing. With this filter, the noise in images is reduced by lowering the quantity of intensity variation between one pixel and its neighbours. Each pixel value in an image is replaced with the average or mean value of its neighbors, including itself [19] as shown in equation 1. Let W_{xy} represent the pixel coordinates in a rectangular sub image window of size m × n centered at point (x, y). The arithmetic mean filtering process computes the average value of the original image g (s, t) of size m×n in the area defined by W_{xy}. The value of filtered image f at any point (x, y) is simply the arithmetic mean computed using the pixels in the region defined by W_{xy}.

$$\hat{f}(x,y) = \frac{1}{mn} \sum_{(s,t)\in W_{xy}} g(s,t) \tag{1}$$

All eliminating pixel values which are unrepresentative of their surroundings are replaced. Since this filter is based on kernel, it is like a convolution filter, in which shape and size of the neighborhood to be sampled is represented when calculating the mean. The more common square kernel is 3 × 3; but bigger kernels such as 5 × 5 squares can be used resulting in more severe smoothing [15]. After testing different sizes of kernels in this study such as 3 × 3, 5 × 5, kernel of size 7 × 7 is used which resulted in more accurate fault detection.

b: MEDIAN FILTER

To preserve useful details in an image, median filter is better than the mean filter. Each pixel is replaced with the median of neighboring pixels. All the pixel values from the surrounding neighborhood are sorted into numerical order and then median is calculated. The pixel being considered is replaced with the middle pixel value as shown in equation 2. Here g(s,t) is the original image, f(x,y) is filtered image and W_{xy} is the window considered.

$$\hat{f}(x,y) = \underbrace{median}_{(s,t)\in W_{x,y}} \{g(s,t)\} \tag{2}$$

It is highly effective for removing noise on images while passing high spatial frequency details. For removal of noise from images corrupted with Gaussian noise, median filter can be less effective [19]. This filter is relatively expensive and complex to compute. All the values in the neighborhood make the processing rather slow [15]. In this case also, after testing various sizes for kernels such as 3 × 3, 5 × 5, kernel of size 7 × 7 is used.

c: GAUSSIAN FILTER

To blur images and remove noise, Gaussian smoothing operator which is a 2-D convolution operator is used. With respect to this, it is like the mean filter but uses a different kernel that represents the shape of a Gaussian (bell-shaped) hump [20]. Gaussian filter is widely used in graphics software for

reduction of image noise by blurring an image. In research areas, it is used as a smoothing operator for blurring the edges. The probability distribution for noise is defined by the gaussian function G(x,y) given by,

$$G(x,y) = \frac{1}{2\pi\sigma^2} e^{-\frac{x^2+y^2}{2\sigma^2}} \quad (3)$$

where σ sigma is the standard deviation of the distribution, x and y are spatial co-ordinates of the pixel in image. The image structures can be enhanced by gaussian smoothing [20]. Typical value of σ =2.5 and kernel of size 7 × 7 is used after trying different values such as 3 × 3, 5 × 5 which improved fault detection efficiency.

d: BILATERAL FILTER

Tomasi [26] proposed Bilateral filter which is a nonlinear filter used to reduce additive noise from images. With nonlinear combination of nearby pixel values, this filter smoothens the images while preserving edge. The bilateral filter, denoted by BF[·], is defined by:

$$BF[I] = \frac{1}{W_p} \sum_{q \in S} G_{\sigma_s}(\|p-q\|) G_{\sigma_r}(|I_p - I_q|) I_q \quad (4)$$

where σ_s and σ_r will specify the amount of filtering for the image I. Normalization factor Wp given by equation 5, ensures pixel weights sum to 1.0:

$$W_p = \sum_{q \in S} G_{\sigma_s}(\|p-q\|) G_{\sigma_r}(|I_p - I_q|) \quad (5)$$

Equation (4) is a normalized weighted average where G_{σ_s} is a spatial Gaussian weighting that decreases the influence of distant pixels, G_{σ_r} is a range Gaussian that decreases the influence of pixels q when their intensity values differ from Ip. Weighted sum of the pixels in a regional neighborhood is considered, which depends on intensity distance and spatial distance [19]. Hence, edges are well preserved, and noise is averaged out. In this study, after testing various values of parameters such as kernel of size 3 × 3, 5 × 5, window size of [5 5] and σ =2.5 and is used.

2) HISTOGRAM EQUALIZATION

Image enhancement is one of the significant and critical issues in low-level image processing. With image enhancement the quality of low contrast images is improved, which increases the intensity difference among objects and background. Contrast enhancement techniques are divided into two methods: Linear and Non-Linear contrast enhancement. In Linear contrast enhancement method contrast stretching is used whereas Non-Linear contrast enhancement method mostly deals with histogram equalizations. Histogram equalization (HE) is the most widely used method which re-assigns the intensity values of pixels resulting in uniform distribution of intensity to highest extent [21].

3) SEGMENTATION

After removal of artifacts from thermal images, fault is localized using two segmentation techniques as mentioned below.

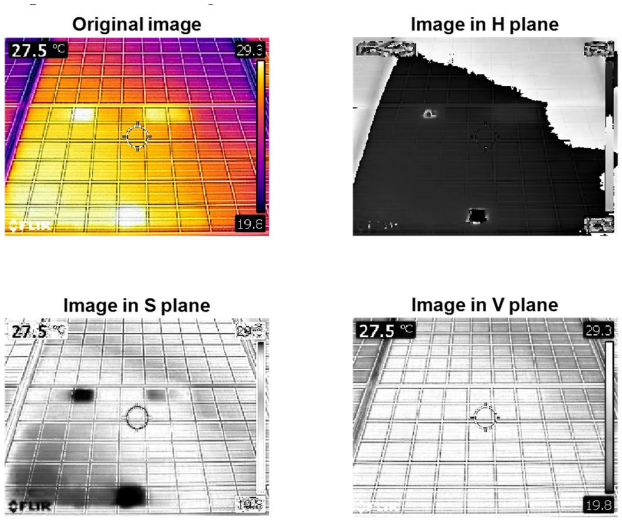

FIGURE 3. Separated channel images for thermal image.

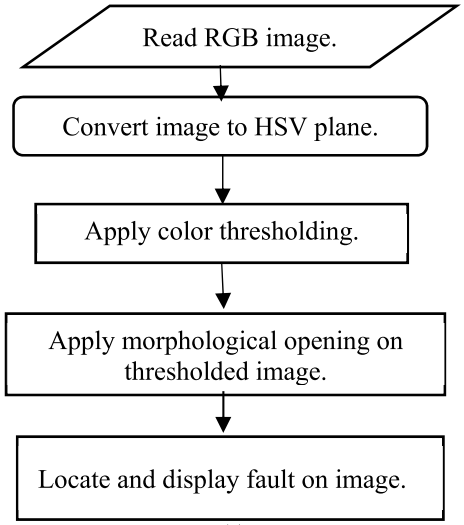

(a)

0	0	0	0	0	0	0	0	0
0	1	1	1	0	1	1	1	0
0	1	1	1	1	1	1	1	0
0	1	1	1	1	1	1	1	0
0	0	0	0	0	0	0	0	0
0	1	1	1	1	1	1	1	0
0	1	1	1	1	1	1	1	0
0	1	1	1	0	1	1	1	0
0	0	0	0	0	0	0	0	0

(b)

FIGURE 4. a) Segmentation based on color thresholding b) Structuring element used in opening operation.

a: SEGMENTATION BASED ON COLOR THRESHOLDING

In this approach, an input RGB image is passed through mean, median, Gaussian, and Bilateral filter separately and then these filtered images are individually converted from RGB plane to HSV plane. As shown in Fig 3., saturation plane prominently indicates the faulty area present in the image.

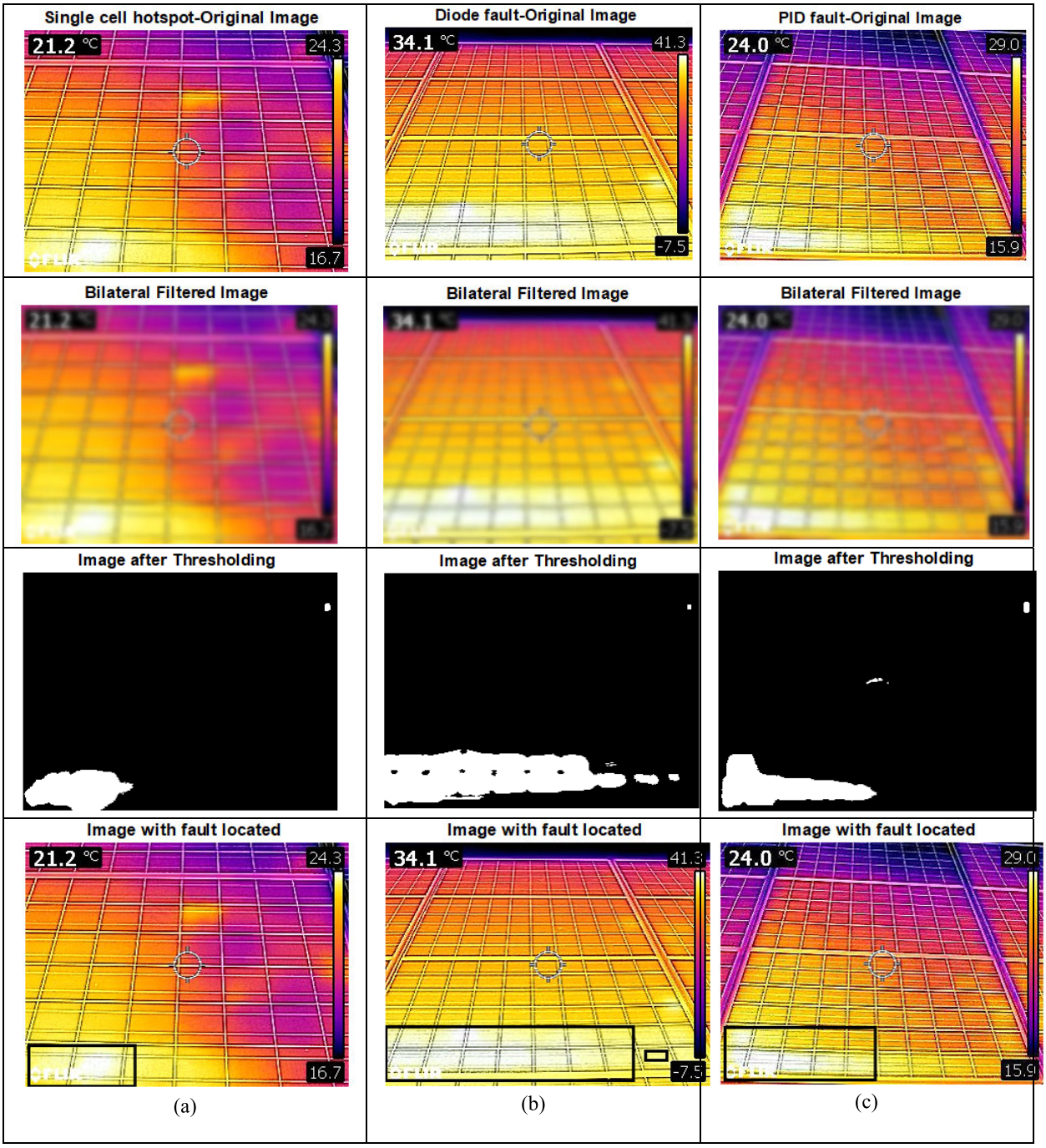

FIGURE 5. Output of various stages as original image, Bilateral filtered image, thresholded image and image with fault located for segmentation based on color thresholding (From top to bottom) (a) Single cell hotspot (b) Diode fault (c) PID fault.

The flowchart for segmentation based on color thresholding is as shown in Fig. 4a.

Using equation 6 to 12 the image is converted from RGB to HSV plane.

Define m and M with the relations,

$$M = max\{R, G, B\} \tag{6}$$

$$m = min\{R, G, B\} \tag{7}$$

And then V and S are defined by the equations,

$$V = M/255 \tag{8}$$

$$S = 1 - m/M \quad if\ M > 0 \tag{9}$$

$$S = 0 \quad if\ M = 0 \tag{10}$$

The hue H is defined by the equations,

$$H = cos^{-1}\left[\frac{(R - 1/2\,G - 1/2B)}{\sqrt{R^2 + G^2 + B^2 - RG - RB - GB}}\right] \quad if\ G \geq B \tag{11}$$

or

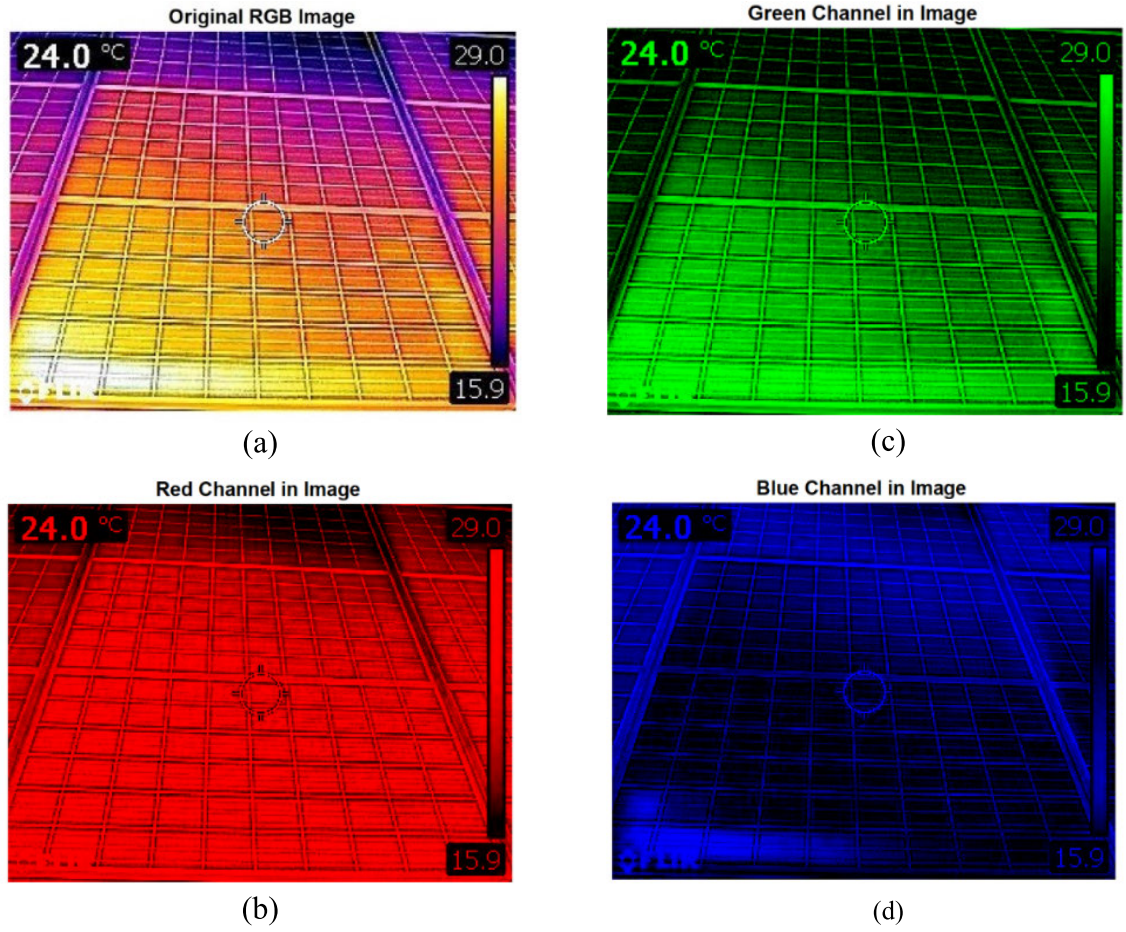

FIGURE 6. Separated channel images for thermal image.

$$H = 360 - cos^{-1}\left[\frac{(R - 1/2\,G - 1/2B)}{\sqrt{R^2+G^2+B^2-RG-RB-GB}}\right] \quad if\ B > G \tag{12}$$

Based onhistogram settingsof HSV channels, threshold value is selected as shown below:

For Hue channel,
0.095<Threshold<0.422
For Saturation channel,
0.000<Threshold<0.455
For Value channel
0.867<Threshold < 1.000

To remove unwanted pixels morphological opening operation is applied on thresholded binary image using the equation 13. The opening of A by B is obtained by taking the union of all translates of B that fit inside A. Parts of A that are smaller than B are removed.

$$A \circ B = \bigcup \{B_x : B_x \subseteq A\} \tag{13}$$

After trying various structuring elements such as disk, square, diamond, cube, sphere, and octagon for opening, specific structuring element (SE) of size 9× 9 as shown in Fig.4b is used during opening operation.

Then on the opened image, fault is located by drawing bounding boxes. Output of various stages of color thresholding is shown in Fig. 5.

b: SEGMENTATION BASED ON SEPARATE COLOR CHANNELS

In this method, the three-color channels are separated from original RGB images. When the images belonging to separate channels are analyzed, it is found that majority of information required for fault detection is present in green and blue channel for thermal images. Red channel of image does not indicate any useful information as shown in Fig. 6.

Based on these results, only green and blue color channels of thermal images are used for thresholding. The flowchart for this approach is as shown in Fig. 7.

Comparing the average values of blue and green channel, either blue or green channel is selected. The selected channel image is converted into gray scale image and total number of pixels are calculated.

$$Th = \left(\frac{total\ no\ of\ pixels}{no\ of\ pixels\ in\ new\ image}\right) * C \tag{14}$$

here C= constant

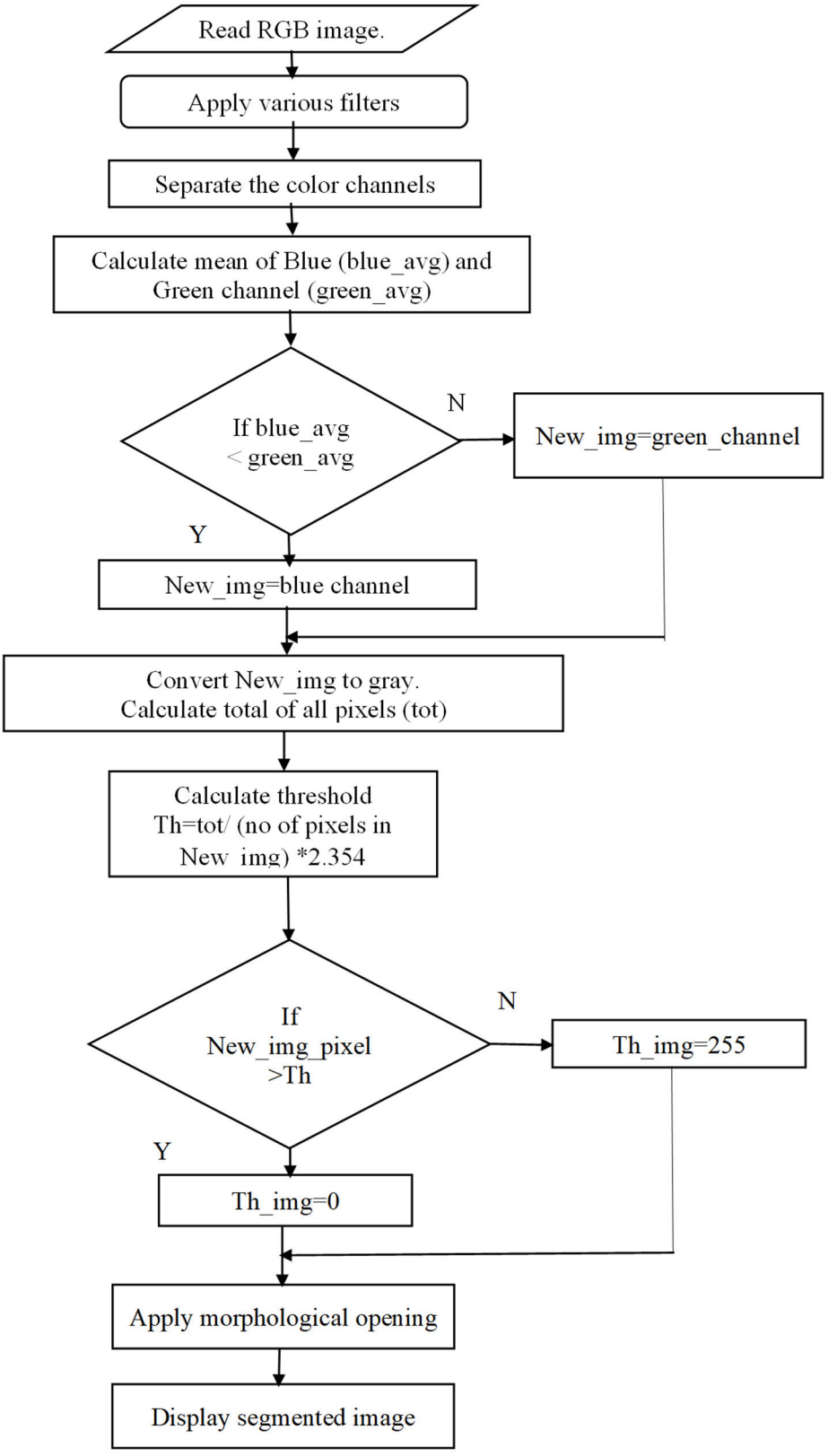

FIGURE 7. Segmentation based on separate color channels.

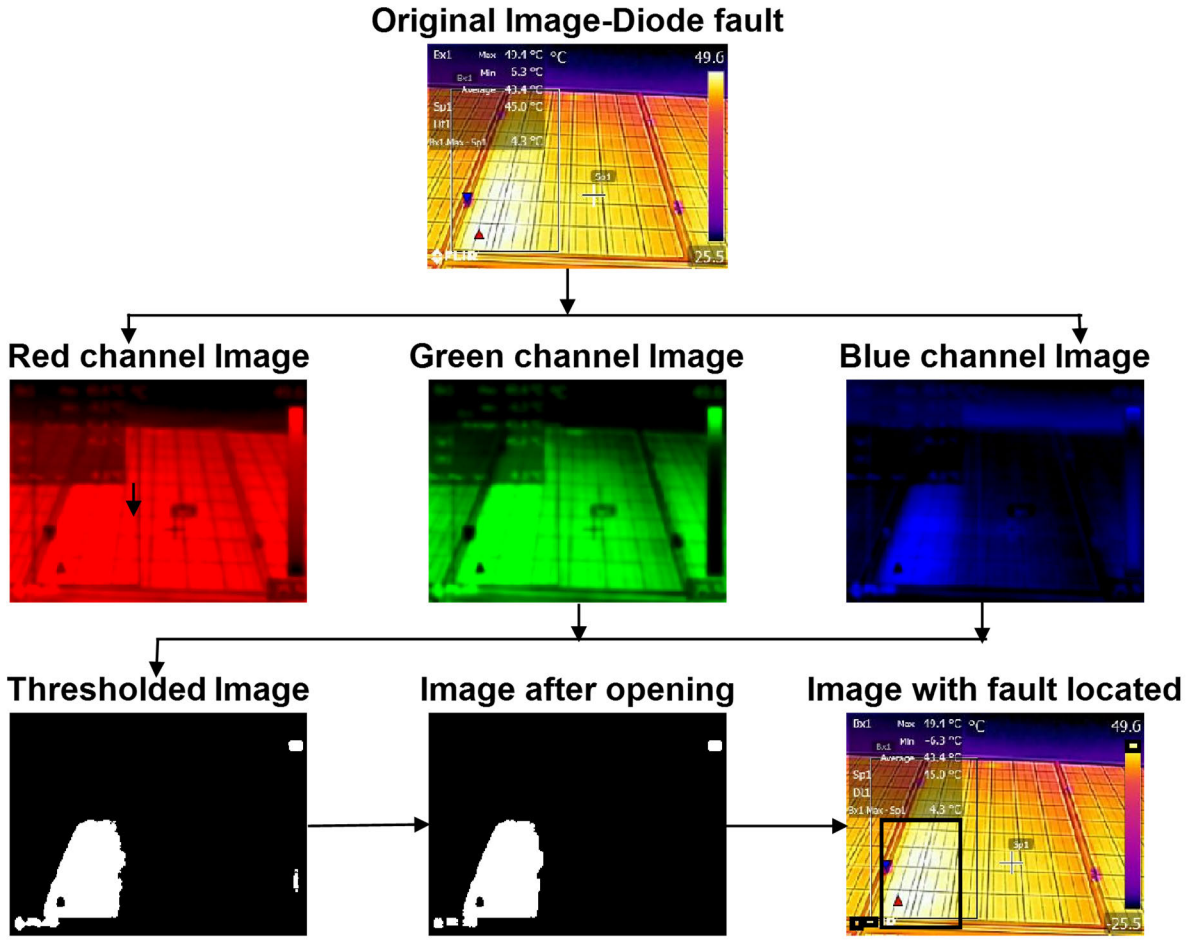

FIGURE 8. Output of various stages as original image (Diode fault), RGB channel images, thresholded image, image after opening and image with fault located for segmentation based on color channel.

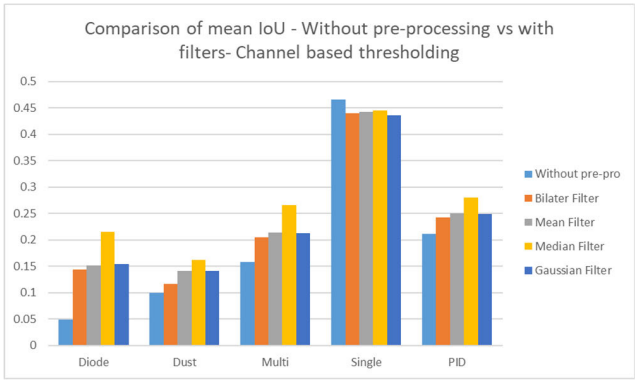

FIGURE 9. Comparison of without pre-processing and with 4 filters using channel-based thresholding.

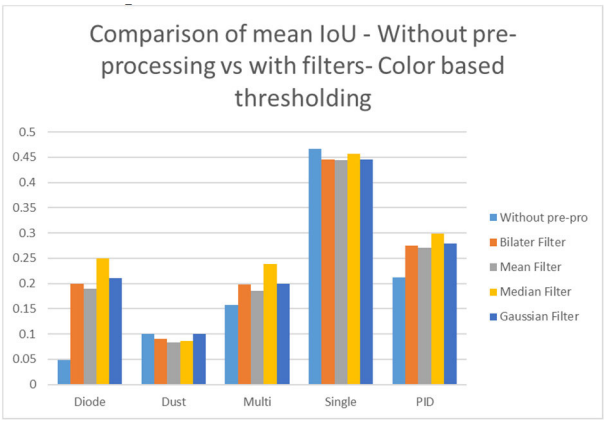

FIGURE 10. Comparison of without pre-processing and with 4 filters using color-based thresholding.

Using equation 14, thresholding is applied on the converted gray scale image with morphological opening and then fault is located. Intersection over Union (IoU) is used as a parameter to compare the performance of proposed methodology for fault detection in thermal images.

Fig.8 shows output of various stages of segmentation using separate color channels for Diode fault. Faults are dominantly seen in green and blue channel image. The fault location is accurately identified in this case of diode fault.

IV. RESULTS AND DISCUSSION

To assess the effect of pre-processing on accuracy of fault detection and demarcation, Intersection over Union (IoU) for

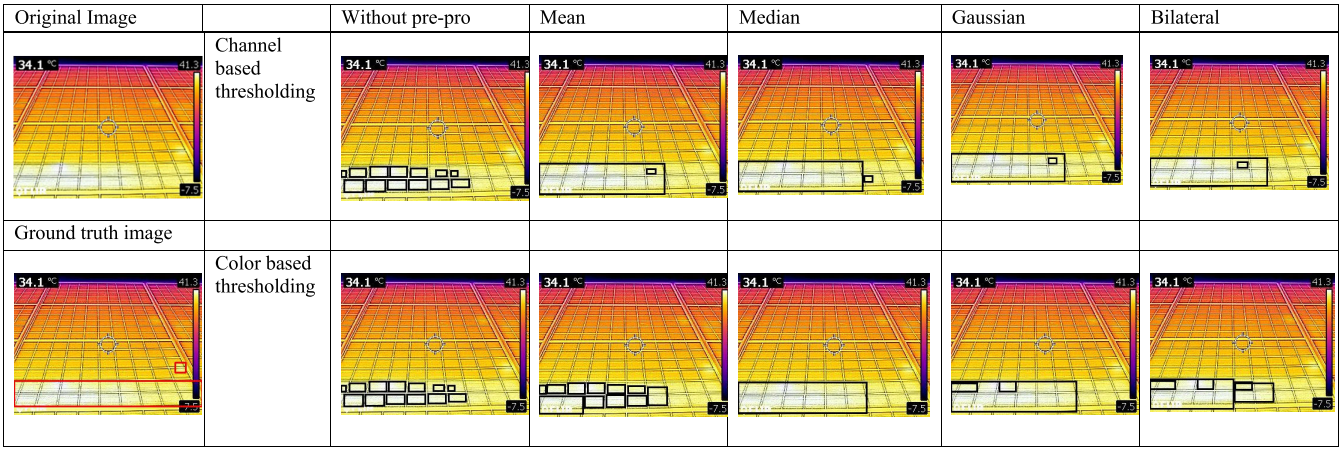

FIGURE 11. Qualitative analysis for fault detection without pre- processing and with 4 filters using channel and color-based thresholding.

TABLE 2. Segmentation results without pre-processing.

	Segmentation results (IoU) based on separate color channels	Segmentation results (IoU) based on color thresholding
Fault	**Mean IoU**	
Diode	0.048707	0.029791
Dust	0.100144	0.062346
Multicell	0.157912	0.119912
Single	0.466396	0.34706
PID	0.211555	0.182733

TABLE 3. Segmentation results based on separate color channels on filtered images.

	Bilateral filter	Mean filter	Median filter	Gaussian filter
Fault	**Mean IoU**			
Diode	0.144148	0.151845	**0.215801**	0.154348
Dust	0.117275	0.142022	**0.161894**	0.142086
Multicell	0.205341	0.213927	**0.266428**	0.212648
Single	0.439561	0.44232	**0.445705**	0.435979
PID	0.242625	0.250927	**0.280037**	0.249695

every image is calculated using Ground Truth (GT) images. Ground truth images are labelled by experts in solar field. Then fault wise average of IoU for all images is calculated. Initially, two proposed segmentation techniques are applied on original thermal images and IoU is calculated as shown in Table 2.

To check the effect of application of filters and pre-processing techniques, various filters and HE is applied on all set of images. Table 3 and Table 4 show results of fault detection algorithm after application of Bilateral, Mean, Median and Gaussian filters. Median filter gave better results

TABLE 4. Segmentation results with histogram based color thresholding on filtered images.

	Bilateral filter	Mean filter	Median filter	Gaussian filter
Fault	**Mean IoU**			
Diode	0.199383	0.189443	**0.249386**	0.210068
Dust	0.091041	0.083581	**0.08639**	0.099608
Multicell	0.197865	0.184977	**0.238425**	0.19906
Single	0.446065	0.443581	**0.457015**	0.445686
PID	0.275508	0.270795	**0.298605**	0.278559

compared to other three filters for both the segmentation approaches. To enhance contrast of filtered images, histogram equalization was applied. Combination of filters and HE was applied on all thermal images and then these images were passed through two segmentation methodologies. When R, G, B channels from thermal image are separated, it is seen that red channel does not show any information related to faulty area.

Using this analysis, segmentation technique based on color channels is applied on all images after filtering and IoU values are calculated as shown in Table 3.

Comparison of IoU values using two segmentation approaches without any pre-processing and with application of four filters is shown in Fig. 9. Mean IoU values are very less which shows the need of pre-processing. Comparing the performance of filters, median filter gives better accuracy for fault detection.

Solar panel thermal images present very dominant color variations in faulty and normal areas of panel. The area with high temperature usually indicated with light color and low temperature area is indicated with purple/blue/red color.

Using this concept of color difference, histogram based color thresholding is applied on filtered thermal images. The results of this technique are shown in Table 4. Graph of histogram based color thresholding without pre-processing

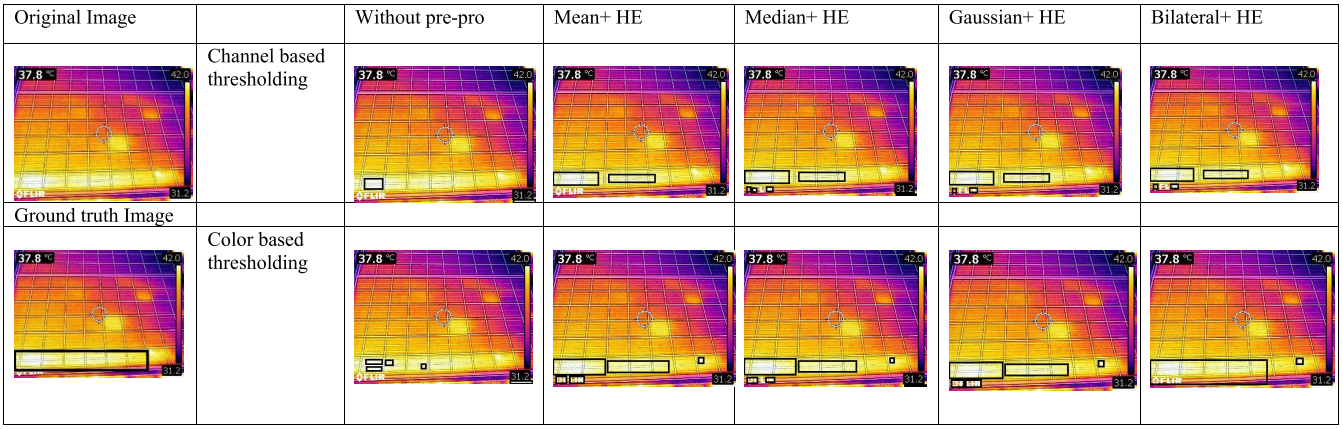

FIGURE 12. Qualitative analysis for fault detection without pre-processing and with 4 filters + HE using channel and color-based thresholding.

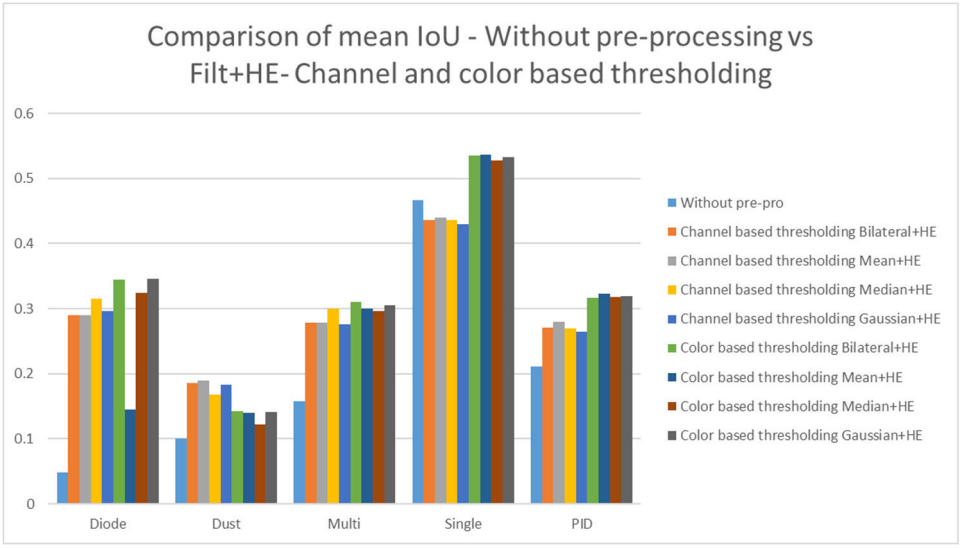

FIGURE 13. Comparison of without pre-processing and with 4 filters + HE using channel and color-based thresholding.

TABLE 5. Mean iou with channel thresholding (FILT+HE).

	Mean+ HE	Med+ HE	Bilat+ HE	Gauss+ HE
Fault types	**Mean IoU**			
Diode	0.29	**0.31535**	0.28988	0.29639
Dust	**0.19**	0.16776	0.18524	0.18288
Multi	0.279	**0.30061**	0.27827	0.27568
Single	**0.4403**	0.43624	0.43630	0.42922
PID	**0.28**	0.2695	0.27030	0.264534

TABLE 6. Mean iou with pre-processing using Segmentation with histogram-based color thresholding.

	Mean+ HE	Med+ HE	Bilat+ HE	Gauss+ HE
Fault types	**Mean IoU**			
Diode	0.3363	0.32439	**0.344511**	0.345654
Dust	0.14	0.12186	**0.142435**	0.141088
Multi	0.3	0.29684	**0.310451**	0.305434
Single	**0.536**	0.52759	0.534702	0.53249
PID	**0.323**	0.31790	0.31673	0.319723

and using four filters is shown in Fig. 10. In this case also median filter performs well.

From Fig. 11, fault detection without any pre-processing applied results in broken segmentation. Median filter gives better results compared to other four filters.

After noise removal using filtering, next step is histogram equalization which is used for image enhancement. Histogram equalization is applied on all filtered images. Two

thresholding techniques as mentioned previously are applied on equalized images and IoU values are calculated.

On the filtered and histogram equalized images, channel-based segmentation and color thresholding is applied and mean IoU for all images is calculated as shown in Table 5.

Results of object detection using two segmentation techniques are shown in Fig. 12 and mean IoU values are shown in Table 6.

Quantitative and Qualitative analysis shows that combination of bilateral filter and HE using color based thresholding gives better results for fault detection.

With filtering and histogram equalization as a pre-processing step, combination of Bilateral filter and histogram equalization gave better results.

To finalise effective pre-processing technique for detection of fault in solar panels, overall values for IoUs with best method from each category are compared, as shown in Fig. 13. Images filtered with Bilateral filter and equalized with HE resulted in better accuracy for fault detection. Due to a smaller number of images in Dust and diode hotspot, average IoU values are less.

With filtering and histogram equalization as a pre-processing step, combination of Bilateral filter and histogram equalization gave better results.

V. CONCLUSION

The amount of power produced by a PV system is limited by a variety of factors such as hotspots, partial shade, diode failure, PV cell failure, and others. The maximum power generation capability of a PV panel is reduced with the increase in severity of the faults in the panel. Early detection of faults in the solar panels is essential to retain the maximum power generation capacity of PV field. Detecting defects with high-definition thermal imaging cameras is an efficient and cost-effective way to ensure a photovoltaic system's long-term profitability.

This paper investigates the need for and effectiveness of pre-processing techniques for fault detection in thermal images. The methodology detects five types of faults: single cell, multicell, diode, dust/shadow, and PID hotspot. Individual performance of four filters, along with histogram equalization, is compared for fault detection. Color thresholding technique based on histograms and thresholding based on separate colour channels are used for segmentation. With the application of four filters on thermal images, the median filter performs well, with higher IoU values than the results without any pre-processing. But in this case, for single cell hot spot, IoU values are more without application of any pre-processing technique. With the combination of filtering and histogram equalization as a pre-processing step, use of bilateral filter in conjunction with the histogram equalisation technique resulted in better accuracy of fault detection in solar panel thermal images. This technique resulted in IoU values of 0.35, 0.14, 0.31, 0.54 and 0.32 for diode, dust, multicell, single cell and PID hotspots respectively. To improve fault detection and demarcation accuracy, efficient segmentation techniques can be used on pre-processed images.

Once the faults are located, they need to be classified into different classes using machine learning or deep learning techniques. In future, techniques may be developed to find the reason behind occurrence of these faults. This research could promote the development of different thermal image applications from different domains.

REFERENCES

[1] M. Sabbaghpur Arani and M. A. Hejazi, "The comprehensive study of electrical faults in PV arrays," *J. Electr. Comput. Eng.*, vol. 2016, pp. 1–10, Dec. 2016, doi: 10.1155/2016/8712960.

[2] J. A. Dhanraj, A. Mostafaeipour, K. Velmurugan, K. Techato, P. K. Chaurasiya, J. M. Solomon, A. Gopalan, and K. Phoungthong, "An effective evaluation on fault detection in solar panels," *Energies*, vol. 14, no. 22, p. 7770, Nov. 2021, doi: 10.3390/en14227770.

[3] B. Basnet, H. Chun, and J. Bang, "An intelligent fault detection model for fault detection in photovoltaic systems," *J. Sensors*, vol. 2020, pp. 1–11, Jun. 2020, doi: 10.1155/2020/6960328.

[4] V. S. B. Kurukuru, A. Haque, and M. A. Khan, "Fault classification for photovoltaic modules using thermography and image processing," in *Proc. IEEE Ind. Appl. Soc. Annu. Meeting*, Sep. 2019, pp. 1–6, doi: 10.1109/IAS.2019.8912356.

[5] C. Henry, S. Poudel, S.-W. Lee, and H. Jeong, "Automatic detection system of deteriorated PV modules using drone with thermal camera," *Appl. Sci.*, vol. 10, no. 11, p. 3802, May 2020, doi: 10.3390/app10113802.

[6] S. Dotenco, M. Dalsass, L. Winkler, T. Würzner, C. Brabec, A. Maier, and F. Gallwitz, "Automatic detection and analysis of photovoltaic modules in aerial infrared imagery," in *Proc. IEEE Winter Conf. Appl. Comput. Vis. (WACV)*, Mar. 2016, pp. 1–9, doi: 10.1109/WACV.2016.7477658.

[7] A. Et-taleby, M. Boussetta, and M. Benslimane, "Faults detection for photovoltaic field based on K-means, elbow, and average silhouette techniques through the segmentation of a thermal image," *Int. J. Photoenergy*, vol. 2020, pp. 1–7, Dec. 2020, doi: 10.1155/2020/6617597.

[8] P. Guerriero and S. Daliento, "Automatic edge identification for accurate analysis of thermographic images of solar panels," in *Proc. 6th Int. Conf. Clean Electr. Power (ICCEP)*, Jun. 2017, pp. 768–772, doi: 10.1109/ICCEP.2017.8004778.

[9] M. Aghaei, F. Grimaccia, C. A. Gonano, and S. Leva, "Innovative automated control system for PV fields inspection and remote control," *IEEE Trans. Ind. Electron.*, vol. 62, no. 11, pp. 7287–7296, Nov. 2015, doi: 10.1109/TIE.2015.2475235.

[10] D. Kim, J. Youn, and C. Kim, "Automatic photovoltaic panel area extraction from UAV thermal infrared images," *J. Korean Soc. Surveying, Geodesy, Photogramm. Cartography*, vol. 34, no. 6, pp. 559–568, Dec. 2016, doi: 10.7848/ksgpc.2016.34.6.559.

[11] E. Kaplani, "Detection of degradation effects in field-aged c-Si solar cells through IR thermography and digital image processing," *Int. J. Photoenergy*, vol. 2012, pp. 1–11, 2012, Art. no. 396792, doi: 10.1155/2012/396792.

[12] H. Jeong, G. R. Kwon, and S. W. Lee, "Deterioration diagnosis of solar module using thermal and visible image processing," *Energies*, vol. 13, no. 11, pp. 1–14, 2020, doi: 10.3390/en13112856.

[13] J. A. Tsanakas, D. Chrysostomou, P. N. Botsaris, and A. Gasteratos, "Fault diagnosis of photovoltaic modules through image processing and Canny edge detection on field thermographic measurements," *Int. J. Sustain. Energy*, vol. 34, no. 6, pp. 351–372, Jul. 2015, doi: 10.1080/14786451.2013.826223.

[14] M. Waqar Akram, G. Li, Y. Jin, X. Chen, C. Zhu, X. Zhao, M. Aleem, and A. Ahmad, "Improved outdoor thermography and processing of infrared images for defect detection in PV modules," *Sol. Energy*, vol. 190, pp. 549–560, Sep. 2019, doi: 10.1016/j.solener.2019.08.061.

[15] J. J. V. Díaz, M. Vlaminck, D. Lefkaditis, S. A. O. Vargas, and H. Luong, "Solar panel detection within complex backgrounds using thermal images acquired by UAVs," *Sensors*, vol. 20, no. 21, pp. 1–16, Sep. 2020, doi: 10.3390/s20216219.

[16] M. Alsafasfeh, I. Abdel-Qader, B. Bazuin, Q. Alsafasfeh, and W. Su, "Unsupervised fault detection and analysis for large photovoltaic systems using drones and machine vision," *Energies*, vol. 11, no. 9, p. 2252, Aug. 2018, doi: 10.3390/en11092252.

[17] D. P. Winston, M. S. Murugan, R. M. Elavarasan, R. Pugazhendhi, O. J. Singh, P. Murugesan, M. Gurudhachanamoorthy, and E. Hossain, "Solar PV's micro crack and hotspots detection technique using NN and SVM," *IEEE Access*, vol. 9, pp. 127259–127269, 2021, doi: 10.1109/ACCESS.2021.3111904.
[18] C.-F. Jeffrey Kuo, S.-H. Chen, and C.-Y. Huang, "Automatic detection, classification and localization of defects in large photovoltaic plants using unmanned aerial vehicles (UAV) based infrared (IR) and RGB imaging," *Energy Convers. Manage.*, vol. 276, Jan. 2023, Art. no. 116495, doi: 10.1016/j.enconman.2022.116495.
[19] X. Wang, W. Yang, B. Qin, K. Wei, Y. Ma, and D. Zhang, "Intelligent monitoring of photovoltaic panels based on infrared detection," *Energy Rep.*, vol. 8, pp. 5005–5015, Nov. 2022, doi: 10.1016/j.egyr.2022.03.173.
[20] S. N. Venkatesh, B. R. Jeyavadhanam, A. M. M. Sizkouhi, S. M. Esmailifar, M. Aghaei, and V. Sugumaran, "Automatic detection of visual faults on photovoltaic modules using deep ensemble learning network," *Energy Rep.*, vol. 8, pp. 14382–14395, Nov. 2022, doi: 10.1016/j.egyr.2022.10.427.
[21] M. S. H. Onim, Z. M. M. Sakif, A. Ahnaf, A. Kabir, A. K. Azad, A. M. T. Oo, R. Afreen, S. T. Hridy, M. Hossain, T. Jabid, and M. S. Ali, "SolNet: A convolutional neural network for detecting dust on solar panels," *Energies*, vol. 16, no. 1, p. 155, Dec. 2022, doi: 10.3390/en16010155.
[22] V. S. B. Kurukuru and A. Haque, "Photovoltaic module fault. Part 1: Detection with image processing approaches," in *Fault Analysis and Its Impact on Grid-Connected Photovoltaic Systems Performance*, 1st ed., A. Haque and S. Mekhilef, Eds. Hoboken, NJ, USA: Wiley-IEEE Press, 2023, pp. 77–110, doi: 10.1002/9781119873785.ch3.
[23] K. C. Liao and J. H. Lu, "Using MATLAB real-time image analysis for solar panel fault detection with UAV," *J. Phys., Conf.*, vol. 1509, no. 1, Apr. 2020, Art. no. 012010, doi: 10.1088/1742-6596/1509/1/012010.
[24] S. Tania and R. Rowaida, "A comparative study of various image filtering techniques for removing various noisy pixels in aerial image," *Int. J. Signal Process., Image Process. Pattern Recognit.*, vol. 9, no. 3, pp. 113–124, Mar. 2016, doi: 10.14257/ijsip.2016.9.3.10.
[25] S. Garg, R. Vijay, and S. Urooj, "Statistical approach to compare image denoising techniques in medical MR images," *Proc. Comput. Sci.*, vol. 152, pp. 367–374, Jan. 2019, doi: 10.1016/j.procs.2019.05.004.
[26] R. M. C. Tomasi, "Bilateral filtering for gray and color images," in *Proc. IEEE Int. Conf. Comput. Vis.*, Jan. 1998, pp. 839–846, doi: 10.1677/joe.0.0930177.

SUJATA P. PATHAK (Member, IEEE) received the M.E. degree in computer engineering from Mumbai University, in 2010.

She is currently an Assistant Professor with the Department of Information Technology, K. J. Somaiya College of Engineering, Somaiya Vidyavihar University, Mumbai, India. She is also a Ph.D. Research Scholar with the Computer Engineering Department, K. J. Somaiya College of Engineering, University of Mumbai. She is also a recognized PG Teacher with the University of Mumbai. She has rich experience of 21 years in teaching. She has supervised many M.Tech. students in information security. She has more than 15 papers in national/international conferences and journals to her credit. Her current research interests include image processing, soft computing, and deep learning. She is a Life Member of the Indian Society of Technical Education (ISTE).

SONALI A. PATIL received the M.E. degree in electronics from the Walchand College of Engineering, Sangli, India, and the Ph.D. degree in technology from Shivaji University, Kolhapur, India. She is currently a Professor with the Department of Information Technology, K. J. Somaiya College of Engineering, Somaiya Vidyavihar University, Mumbai, India, where she also owns the responsibility of the Associate Dean of academic programs. She is recognized as the PG Teacher and the Ph.D. Supervisor/Guide of the University of Mumbai and Somaiya Vidyavihar University. She has rich experience of more than 19 years in teaching and one year in industry. She has supervised many M.Tech. students in the area of information security and computer engineering. She has publications in peer-reviewed international journals, book chapters, and conferences in the areas of information security and image processing. Her current research interest includes GIS, Image processing and analysis.